Physics of Fluids

Experimental investigation of interactions between turbulent cylinder wake and spherical shock wave

Cite as: Phys. Fluids **32**, 016101 (2020); https://doi.org/10.1063/1.5128267
Submitted: 18 September 2019 . Accepted: 10 December 2019 . Published Online: 02 January 2020

Kenta Aruga, Kento Inokuma, Tomoaki Watanabe, Koji Nagata, and Yasuhiko Sakai

Physics of Fluids ARTICLE scitation.org/journal/phf

Experimental investigation of interactions between turbulent cylinder wake and spherical shock wave

Cite as: Phys. Fluids 32, 016101 (2020); doi: 10.1063/1.5128267
Submitted: 18 September 2019 • Accepted: 10 December 2019 •
Published Online: 2 January 2020

Kenta Aruga,[1] Kento Inokuma,[1] Tomoaki Watanabe,[1,a)] Koji Nagata,[1] and Yasuhiko Sakai[2]

AFFILIATIONS

[1]Department of Aerospace Engineering, Nagoya University, Nagoya, Japan
[2]Department of Mechanical Systems Engineering, Nagoya University, Nagoya, Japan

[a)]watanabe.tomoaki@c.nagoya-u.jp

ABSTRACT

Interactions between a spherical shock wave and a turbulent cylinder wake are studied with wind tunnel experiments. The shock wave is generated outside the wake and propagates across the turbulent wake. Instantaneous streamwise velocity is measured on the wake centerline while peak overpressure of the shock wave is measured outside the wake after the shock wave has passed across the wake. The experiments are performed for various conditions of the cylinder wake to investigate the influences of the root-mean-squared (rms) velocity fluctuation and of the length of the turbulent region through which the shock wave propagates. The velocity fluctuation opposite to the shock propagation direction is positively correlated with the peak-overpressure fluctuation. The mean peak overpressure decreases after the shock wave propagates in the wake. These relations between velocity and peak overpressure are explained by the shock-surface deformation, where the peak overpressure is increased and decreased, respectively, for the shock surfaces with concave and convex shapes in relation to the shock propagation direction. The correlation coefficients between the velocity and peak-overpressure fluctuations and the rms peak-overpressure fluctuation increase with the rms velocity fluctuation. The rms peak-overpressure fluctuation becomes independent of the turbulent length on the shock ray once the shock wave has propagated through a sufficiently long turbulent region. The peak-overpressure fluctuation has a probability density function (PDF) close to a Gaussian shape even though the PDF of velocity fluctuations in the wake is negatively skewed.

I. INTRODUCTION

Interactions between a shock wave and turbulence can be found in various scientific problems. For example, the sonic boom caused by the shock wave induced by supersonic flight propagates through atmospheric turbulence. The interaction of the shock wave with atmospheric turbulence alters the pressure waveform observed on the ground.[1] Because the pressure waveform is directly related to the noise level of the sonic boom, the interaction between the shock wave and atmospheric turbulence is considered an important factor in the prediction of a sonic boom.[2–4] Understanding the mechanism of the interaction between the shock wave and turbulence is expected to contribute to sonic boom prediction. Propagation of the shock wave in turbulence affects the strength of the shock wave, i.e., shock Mach number, which is an important parameter in flows with shock waves. Therefore, in addition to the importance of the shock/turbulence interaction in engineering fields, it also plays important roles in physics problems such as in star formation by supernova explosion[5] and inertial confinement fusion.[6]

Shock/turbulence interactions have been studied in theories, experiments, and numerical simulations. From the view point of turbulence, various theories and models have been developed for homogeneous turbulence because the assumption of statistical homogeneity results in a relatively simple description by governing equations of statistics.[7,8] Similarly, many theoretical studies of shock/turbulence interaction also deal with homogeneous turbulence.[9–14] Numerical simulations have also been performed for the interaction between a normal shock wave and homogeneous turbulence (homogeneous in the shock tangential directions).[9,11,15–19] Similarly, experiments have been conducted to study the interaction between shock waves and grid-generated turbulence, which is often considered as a good approximation of decaying

homogeneous isotropic turbulence.[20–22] These previous studies have found changes in the characteristics of both shock wave and turbulence by the interaction.

In most practical problems, however, turbulence is statistically inhomogeneous, where statistics are dependent on positions in a flow. For example, the sonic boom is influenced by atmospheric boundary layers, whose characteristics significantly vary in the vertical direction.[23] Free shear flows, such as jets, mixing layers, and wakes, are canonical inhomogeneous turbulent flows and have been studied to investigate turbulence from many aspects. These flows have a large mean velocity gradient in the transverse direction, which results in the production of turbulent kinetic energy. A shock wave interacting with a jet was studied with a conical shock tube, where the shock wave propagates in the same or opposite direction of the jet.[24] They confirmed that the pressure jump by the shock wave is intensified when the shock propagation direction is opposite to the jet direction and vice versa. Kim *et al.* investigated turbulent effects on overpressure behind a blast wave interacting with a turbulent jet,[25] where the shock wave propagates in the transverse direction of the jet. They found that both average and root-mean-squared (rms) fluctuation of the peak overpressure change by the interaction with the turbulent jet.

An important feature of free shear flows is outer intermittency: At a fixed location in the flow, both turbulent and nonturbulent (laminar) fluids can be observed depending on time.[7] The flow characteristics are very different between the turbulent and nonturbulent regions.[26–31] Since the turbulent fluid has stronger velocity fluctuations than the nonturbulent fluid, it is expected that the spatial distribution of turbulent fluids is important in the shock wave propagating through free shear flows. For example, the shock waves are generated inside a high-speed turbulent mixing layer and propagate outward from the mixing layer.[32–34] This propagation of the shock waves can also be influenced by the intermittent turbulent profile of the mixing layer. The spatial distribution of turbulent fluids can also be important in interactions between shock waves and turbulent boundary layers.[35,36] Numerical simulations found that once the shock wave begins to propagate through turbulence, the rms fluctuation of the pressure jump across the shock wave gradually increases.[18] This result also indicates the importance of the spatial distribution of turbulence when the shock wave propagates through intermittent turbulent flows. Even though inhomogeneity of turbulence is expected to be important in the interaction between the shock wave and turbulence, the shock wave propagating in inhomogeneous turbulence has not been studied in a systematic manner in previous studies.

In this study, wind tunnel experiments are conducted for the interaction between a spherical shock wave and a turbulent cylinder wake, which is produced by a cylinder placed in the freestream. The shock wave propagates from the laminar freestream region to the turbulent cylinder wake and passes across the turbulent region to the laminar freestream in another side of the wake. In the experiments, the velocity fluctuation in the wake and overpressure behind the shock wave are measured. The experiments are performed to investigate the turbulent effects on the shock wave in terms of the rms velocity fluctuation and the length of the turbulent region through which the shock wave propagates. The interaction between shock waves and turbulence in physics and engineering problems is far more complicated than in laboratory experiments. However, in this study, a series of experiments conducted under idealized conditions are useful for identifying the factors that influence the interaction. The present experiments are designed to study the effects of statistical inhomogeneity in the turbulent velocity field.

This paper is organized as follows: The details of the experiments are presented in Sec. II, where the experimental setup and methods of statistical analysis are presented. Section III presents the experimental results: the fundamental characteristics of the turbulent cylinder wakes, the statistics of the peak overpressure of the spherical shock wave interacting with the wake, and the relation between the velocity fluctuation in the wake and the peak overpressure of the shock wave. Finally, the conclusion is presented in Sec. IV.

II. WIND TUNNEL EXPERIMENTS

A. Experimental apparatus

We conduct wind tunnel experiments of the interaction between the turbulent cylinder wake and the spherical shock wave. The experimental setup is shown in Fig. 1. The experiments are conducted with a closed-loop wind tunnel whose test section with a streamwise length of 4000 mm has a cross section of 994 mm × 460 mm. The detail of the wind tunnel can be found in Ref. 37. The shock wave generator was developed in Ref. 21 and has also been used in our previous studies.[22,38,39] The shock wave is generated in a shock tube with a quick piston valve, which releases compressed air at 900 kPa into air at atmospheric pressure. The shock wave propagates through the tube whose open end is connected to the wind tunnel. The shock wave is ejected vertically downward from the open end of the tube into the test section and forms the spherical shock wave. The cylinder wake is generated by installing an aluminum

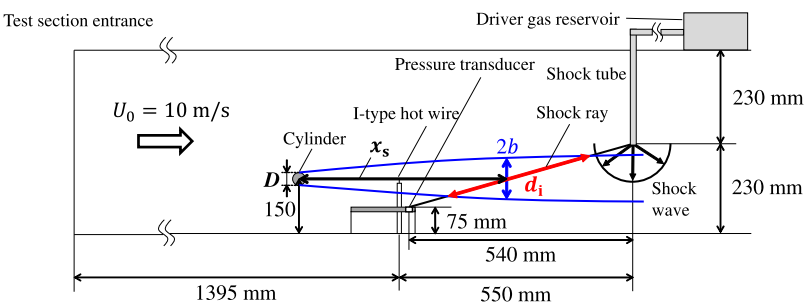

FIG. 1. Schematic of experiments of the interaction between a spherical shock wave and a cylinder wake.

hollow cylinder with a diameter D = 5, 10, 12, 15, or 20 mm inside the test section. The cylinder has the same length as the width of the test section and is horizontally placed in the test section.

The overpressure and streamwise velocity are measured with a pressure transducer (PCB Piezotronics, Inc., 113B27) and a hot-wire anemometer (DANTEC StreamLine with an I-type probe, DANTEC 55P11), respectively. The hot-wire anemometer has been widely used to measure velocity in turbulent free shear flows,[40] such as wakes, jets, and mixing layers, where the turbulent intensity can exceed 10%. Previous studies of turbulent jets showed that velocity statistics obtained with hot-wire anemometry agree well with those with direct numerical simulations (DNSs) and other measurement methods.[41–43] The pressure transducer and the hot-wire probe are installed on a measurement plate near the bottom wall of the wind tunnel. The plate is installed at a height of 75 mm from the bottom wall to prevent a boundary layer on the bottom wall of the wind tunnel from affecting the pressure measurement.[38] The pressure transducer is mounted flush with the wall, which is horizontally placed in the test section. The wall has the same spanwise length as that of the test section. The cylinder is placed so that the cylinder wake develops at the height between the open end of the shock tube and the pressure measurement location. This arrangement enables us to measure the pressure jump caused by the shock wave that has propagated through the cylinder wake. The shock Mach number M_S at the pressure measurement location is 1.004 at a freestream velocity of 10 m/s without the wake. A computer controls the shock generator and measurements, where signals from the pressure transducer and hot-wire anemometer are recorded at a sampling rate of 1 MHz with an oscilloscope (YOKOGAWA DL850E). The measurement of overpressure and velocity starts before the shock wave is ejected, and this allows us to estimate the velocity fluctuation that affects the overpressure of the shock wave measured at the pressure transducer location, as described in Sec. II C. The details of these measurement methods can also be found in Ref. 38.

In all experiments, the streamwise distance between the pressure transducer and the open end of the tube of the shock wave generator is fixed as 540 mm. The vertical distance of the cylinder position from the wall is also fixed at 150 mm. On the other hand, the streamwise position of the cylinder is changed in each experimental condition. The overpressure measured by the pressure transducer is strongly influenced by turbulence on the shock ray between the open end of the shock tube and the pressure transducer position.[18,38] Since the cylinder wake develops in the streamwise direction, one of the important parameters in the experiments is the streamwise distance from the cylinder to the shock ray denoted by x_s in Fig. 1.

The experiments are conducted for eight sets of (x_s, D) with freestream velocity U_0 = 10 m/s. One of the main purposes of this study is to investigate the shock/turbulence interaction in terms of the length of turbulent regions through which the shock wave propagates. It is useful to estimate the wake core region as twice the half-width b based on the mean velocity defect, which is defined as the mean velocity difference from the freestream velocity. Note that the outer region of the wake is highly intermittent in the sense that both turbulent and nonturbulent fluids appear at a certain location.[7] Prior to the experiments of the shock/turbulence interaction, we have measured the streamwise evolution of the half-width b. Based on the shock ray and the distribution of the wake core region, the length d_i over which the shock wave propagates within the wake core region is obtained and shown in Fig. 1. In this paper, d_i is called an interaction length. Table I summarizes the experimental conditions, where (x_s, D) are chosen based on the streamwise rms velocity fluctuation u_{rms} and the interaction length d_i. Here, the statistics of the cylinder wake are computed with time average and obtained from experiments conducted independently from the shock/turbulence interaction experiments. u_{rms} is taken at the streamwise distance of x_s away from the cylinder (the streamwise position where the shock ray intersects the centerline of the cylinder wake). Cases 1–4 have $d_i \approx 200$ mm while u_{rms} is different for each case. These experiments are used to investigate the influence of u_{rms} for a fixed value of d_i. On the other hand, d_i is different but $u_{rms} \approx 0.5$ m/s is similar for case 1 and cases 5–9. Table I also includes the integral length scale L_u computed by integrating the autocorrelation function of streamwise velocity fluctuation and the mean velocity defect on the centerline, U_{def}, at the streamwise distance of x_s away from the cylinder.

In addition to the experiments on the interaction of the shock wave and cylinder wake, experiments are also performed for the shock wave propagating through grid turbulence or a laminar flow. The grid turbulence is generated by installing a square grid with a mesh size of M = 100 mm at the entrance of the test section. The grid turbulence in this wind tunnel was also studied in Ref. 37. The experiment for the laminar flow is conducted without installing the grid or the cylinder. In these experiments, the velocity is also measured at the same position as in the experiments for the cylinder wake. Note

TABLE I. Experimental conditions.

Case	D (mm)	x_s (mm)	x_s/D	b (mm)	d_i (mm)	u_{rms} (m/s)	L_u (mm)	d_i/L_u	U_{def} (m/s)	τ_e/τ_{adv}
1	10	750	75.0	25.8	200	0.511	57.6	3.48	1.16	4.35
2	5	1500	300	22.7	208	0.203	62.3	3.34	0.645	11.8
3	12	654	54.5	26.1	201	0.658	66.1	3.03	1.33	3.85
4	15	565	37.6	27.7	201	0.870	68.3	2.94	1.67	3.04
5	5	285	57.0	10.6	85.8	0.539	13.2	6.51	1.23	0.92
6	12	900	75.0	31.6	240	0.529	72.2	3.33	1.16	5.23
7	15	1161	77.4	42.2	305	0.539	98.8	3.09	1.10	7.04
8	20	1500	75.0	53.5	400	0.512	126	3.18	1.08	9.46
9	Grid turbulence			...	562	0.549	52.8	10.6	...	21.1

that the laminar flow also has a small but nonzero rms velocity fluctuation that is inherent in the wind tunnel, where the laminar flow with $U_0 = 10$ m/s has $u_{rms} = 0.05$ m/s.

B. Analysis of peak overpressure of shock wave

Figure 2 shows an example of the time history of the overpressure p and velocity u. The shock wave causes a distinct jump in the overpressure. After the overpressure reaches a peak, it gradually decreases with time because of the expansion wave propagating behind the shock wave. The second peak appears around 220 μs due to the reflection of the shock wave in the wind tunnel. Except for this second peak, the typical pressure waveform of the spherical shock wave is obtained in this experiment. Although the velocity is measured in the turbulent wake, the velocity fluctuations before the shock arrival look very small in Fig. 2. This is because the time scale of large-scale velocity fluctuations of the wake is of the order of 10^2 ms, which is much longer than the time scale of the horizontal axis of Fig. 2. As the overpressure increases by the shock wave, the velocity rapidly decreases because of the induced velocity of the shock wave. Then, the velocity gradually increases as the expansion wave propagates behind the shock wave. Temperature also changes by the shock wave. The induced velocity and temperature fluctuations can result in errors in velocity measurement by the hot-wire anemometer. However, as explained below, we only use the velocity signal recorded before the shock ejection, and the statistics presented in this paper are not influenced by the velocity measurement errors due to the shock wave. For each condition, experiments are repeated 500 times, and 500 sets of time-series data are obtained for overpressure and velocity. The statistical analysis is conducted based on an ensemble average of 500 datasets denoted by $\langle\cdot\rangle$. The peak overpressure, Δp, can be defined with the peak in the overpressure, as shown in Fig. 2.

The angle between the measurement plate and the shock ray toward the pressure transducer is 16°. The effect of the angle on Δp is investigated by additional experiments conducted with various pressure transducer locations. Hereafter, θ is defined as the angle of the shock ray from the vertically downward direction. The plate is horizontally placed in the wind tunnel in all experiments while vertical and horizontal locations of the plate are determined so that Δp can be measured for different θ with a fixed distance R between the pressure transducer and the open end of the shock tube. Here, the distance R is the same as in other experiments conducted in this study. These experiments provide Δp as a function of θ. An empirical relation between Δp and θ for the regular reflection of a weak shock wave[44] ($M_S \to 1$) is written as

$$\Delta p(\theta) = 0.5\Delta p(0^\circ)(1 + \cos\theta). \quad (1)$$

Figure 3 compares $\Delta p(\theta)$ with Eq. (1), where $\Delta p(0^\circ)$ is also obtained by the experiment. The measurement results agree well with Eq. (1), confirming that θ-dependence of Δp in our experiments is well explained by the regular reflection. Equation (1) would not be valid if the reflection on the measurement plate were influenced by complex reflection phenomena such as Mach reflection, in which the geometry of the incident and reflected shock waves is different from that of the regular reflection.[45] For all experiments in this study, θ is 74°, and the present experiments measure the peak overpressure of the shock wave with the regular reflection on the measurement plate.

In this study, we analyze the effects of turbulence on the statistical properties of Δp. There are several sources of errors in Δp measured by the pressure transducer in wind tunnel experiments. Sasoh *et al.* analyzed the errors in Δp of the shock wave interacting with turbulence in wind tunnel experiments and proposed a procedure to evaluate the effects of turbulence on rms fluctuation of Δp.[21] We briefly discuss this procedure below and further details can be found in Ref. 21. The peak-overpressure fluctuation has a nonzero rms value, $\sqrt{\langle\Delta p^2\rangle - \langle\Delta p\rangle^2}$, even when the shock wave is ejected in a quiescent fluid. This fluctuation is inherently caused by the experimental facility and measurement system (e.g., electrical noise) independently of turbulent flows. The latter one is evaluated by computing the rms value of overpressure fluctuation without the shock wave $\sigma_N(U_0) = \sqrt{\langle p^2\rangle_t - \langle p\rangle_t^2}$, where the time average is denoted by $\langle\cdot\rangle_t$. Since σ_N slightly depends on the freestream velocity U_0, σ_N is measured for $U_0 = 0$ and 10 m/s in this study. The spherical shock wave produced by the shock wave generator also has a non-negligible fluctuation in Δp. The contribution of this fluctuation to $\sqrt{\langle\Delta p^2\rangle - \langle\Delta p\rangle^2}$ can be estimated by the

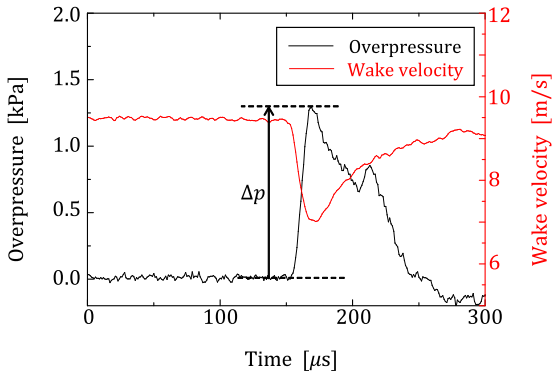

FIG. 2. Time history of overpressure and velocity measured in case 1.

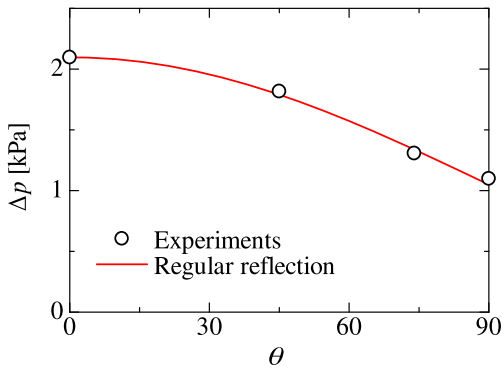

FIG. 3. Dependence of peak overpressure on the angle between the plate and the shock ray. Here, θ is the angle between the vertically downward direction and the shock ray toward the pressure transducer, where the plate is horizontal to the wall. The relation for the regular reflection [Eq. (1)] is also shown for comparison.

overpressure measurement of the shock wave ejected in a quiescent fluid ($U_0 = 0$ m/s) as $\sigma_S = \sqrt{\langle \Delta p^2 \rangle - \langle \Delta p \rangle^2 - \sigma_N^2(0)}$. It can be assumed that the fluctuations contributing to σ_S and σ_N are independent of the influence of turbulence on the shock wave. Then, the influence of turbulence on the peak-overpressure fluctuation is evaluated as

$$(\Delta p_{rms})_T = \sqrt{\langle \Delta p^2 \rangle - \langle \Delta p \rangle^2 - \sigma_S^2 - \sigma_N^2} \quad (2)$$

with σ_N measured at $U_0 = 10$ m/s.

C. Correlation between peak overpressure of shock wave and velocity fluctuation

The correlation between the peak-overpressure fluctuation and the velocity fluctuation is calculated using the same method as in Ref. 38. The hot-wire probe measures the velocity on the wake centerline, which is different from the pressure measurement location. Previous studies of spatial and temporal correlation of turbulent velocity and pressure jump of the shock wave showed that a pressure jump fluctuation at one point on the shock wave is not strongly correlated with the velocity at the same point.[18,38] A strong correlation is found for the velocity in the region where the shock wave has already passed. In other words, once the shock wave interacts with the velocity fluctuation at one point, this interaction causes the pressure-jump fluctuation after the shock wave propagates for a certain distance close to the integral length scale.[18,38] In the present experimental setup, the peak overpressure on the wall is expected to be strongly correlated with the velocity on the ray away from the pressure transducer. Therefore, it is important to measure the velocity above the pressure transducer. Here, the hot-wire probe is installed to measure velocity on the wake centerline, whose correlation with the peak overpressure is investigated with the procedure described below.

The interaction between the shock wave and wake is studied in terms of the interaction length d_i and rms velocity fluctuation u_{rms}. The streamwise velocity is measured using a hot-wire probe, while the shock ray toward the pressure transducer has an angle of 16° with the streamwise direction. This angle is partially taken into account by introducing the interaction length d_i, which depends on the angle between the shock ray and the streamwise direction. From previous DNS studies, it was shown that the velocity in the shock normal direction, U_n, is important in the peak-overpressure fluctuation caused by the interaction. In the present experiments, U_n can be written as $U_n = U\cos(16°) + V\sin(16°)$, where U and V are the streamwise and vertical components of the velocity vector, respectively. Because of the small angle, the shock normal component is often dominated by U. $U_n \neq U$ might have influences on the results plotted against u_{rms} and the correlation coefficient between the peak-overpressure fluctuation and velocity fluctuation. However, the correlations obtained in this study qualitatively agree with the DNS of the shock wave propagating in isotropic turbulence, where the correlation was calculated with the shock normal velocity.[18] Further quantitative discussions require measurements of the shock normal velocity.

The correlation analysis uses the signals from the hot-wire anemometer recorded before the shock wave ejection. It should be noteworthy that the velocity measured after the shock wave ejection is influenced by the shock wave. For example, the induced velocity by the shock wave is also measured by the hot-wire anemometer when the shock wave reaches the probe location. Temperature correction may be necessary in order to measure the velocity of turbulence that has interacted with the shock wave because the shock wave also affects temperature. However, as long as the signals recorded before the shock ejection are concerned, the velocity measured by the hot-wire anemometer is not influenced by the shock wave.

The characteristic velocity of the cylinder wake with the freestream velocity of 10 m/s is much smaller than the shock propagation speed. Therefore, with Taylor's frozen turbulence hypothesis, the time series data $U(t)$ can be used to estimate the instantaneous streamwise profile of the velocity at the instance of the shock wave ejection. The convection velocity of the wake can be calculated as $U_{con} = (U_0 + U_c)/2$, where U_c is the mean velocity on the centerline calculated with time average without the shock wave. The convection velocity U_{con} obtained in this definition shows good agreement with Ref. 46, and U_{con} hardly depends on its definition because the velocity defect is small. For each experiment, t is defined as time elapsed after the peak overpressure is observed in the pressure signal. Hereafter, d is defined as the streamwise distance from the pressure transducer. $U(d)$ at the height of the hot-wire probe is obtained from $U(t)$ with $d = -U_{con}t - \Delta_{HP}$, where $\Delta_{HP} = 10$ mm is the streamwise distance between the hot-wire probe and the pressure transducer. The velocity profile $U(d)$ between the streamwise locations of the pressure transducer and shock tube (0 mm $\leq d \leq$ 540 mm) is calculated from the velocity signal recorded before the shock wave ejection ($t < 0$). For investigating scale dependence of turbulence, a low-pass filter is applied for $U(t)$ as $\overline{U}(t, \Delta t) = (1/\Delta t)\int_{t-\Delta t/2}^{t+\Delta t/2} U(\tau)d\tau$ with a cutoff time scale Δt, which can be converted to the spatial length scale $\Delta d = U_{con}\Delta t$ with the Taylor hypothesis. These manipulations of the signal yield the low-pass filtered velocity $\overline{U}(d, \Delta d)$. Δd represents the length scale in the streamwise direction. The same method has often been used in spectral analysis, where frequency is converted to wavelength.[41,42]

The peak-overpressure fluctuation $\Delta p' = \Delta p - \langle \Delta p \rangle$ and low-pass filtered velocity fluctuation $\overline{U}' = \overline{U}(d, \Delta d) - U_c$ are obtained for every ejection of the shock wave. The correlation coefficient $R(d, \Delta d)$ between $\Delta p'$ and $\overline{U}'(d, \Delta d)$ is defined based on an ensemble average as

$$R(d, \Delta d) = \frac{\langle \overline{U}' \Delta p' \rangle}{\sqrt{\langle \overline{U}'^2 \rangle \langle \Delta p'^2 \rangle}}. \quad (3)$$

The streamwise velocity fluctuation is defined to be positive in the streamwise direction while the shock wave propagates in the opposite direction.

Application of the Taylor hypothesis requires that the turbulence evolves more slowly than the advection by the mean flow. The advection time scale τ_{adv} of the wake with the freestream velocity 10 m/s over the streamwise distance 271 mm between the hot-wire and the shock ray toward the pressure transducer is 0.027 s. Table I shows the eddy turnover time of large-scale turbulent motions $\tau_e = L_u/u_{rms}$ divided by τ_{adv}. In most cases, τ_e is greater than τ_{adv}, indicating that the large-scale turbulent motions are slower than the mean flow advection. However, case 5 has $\tau_e/\tau_{adv} \approx 1$, for which the turbulence advects itself significantly over time τ_{adv}. Therefore,

except for case 5, the analysis based on the Taylor hypothesis is applied.

III. RESULTS AND DISCUSSION

A. Statistics of cylinder wake

The streamwise evolution of the wake from the cylinder with D = 10 mm is presented in Fig. 4 based on the velocity measurement, where x denotes the streamwise distance from the cylinder center. Figure 4(a) shows a streamwise distribution of $u_{\rm rms}/U_0$. It is known that $u_{\rm rms}$ decays following a power law[47] $u_{\rm rms}/U_0 = C(x/D - x_0/D)^{-n}$. The least squares method yields $C = 0.62$, $x_0/D = 6.5$, and $n = 0.58$ for the present results. Figures 4(b) and 4(c) show Taylor microscale λ and integral length scale L_u against $(x - x_0)/D$ on the wake centerline. Here, the Taylor microscale is calculated as $\lambda = u_{\rm rms}/(du/dx)_{\rm rms}$ based on the spatial derivative estimation with the Taylor hypothesis. These length scales also increase in the streamwise direction following power laws. We obtain $\lambda/D = 0.12(x/D - 6.5)^{0.31}$ and $L_u/D = 0.42(x/D - 6.5)^{0.58}$ by the least squares method with the virtual origin obtained for $u_{\rm rms}$. The exponents of the power laws for λ and L_u are close to the values obtained in previous experiments.[47]

Figure 5 shows frequency power spectra $E(f)$ of the streamwise velocity fluctuations on the wake centerline for all cases, where the hot-wire probe is installed on the measurement plate as in the experiments of the interaction between the shock wave and the cylinder wake. Peaks associated with Karman vortices cannot be seen in the power spectra for all cases. There is a range for which the power spectra follow Kolmogorov's $k^{-5/3}$ law shown with the dashed-dotted line. These results confirm that the turbulent cylinder wake has reached a fully developed state before it interacts with the shock wave.

Figure 6(a) shows probability density functions (PDFs) of streamwise velocity fluctuation u' in the cylinder wake at different transverse locations y, where y is defined as the vertical distance from the center of the cylinder wake. Figure 6(b) shows the skewness and flatness of u'. The PDFs of streamwise velocity fluctuation at $y/b = 0$ and 0.5 are close to the Gaussian function, for which the skewness and flatness are 0 and 3, respectively. These values for the Gaussian PDF of a variable f, $P(f)$, can be obtained by calculating averages of f^2, f^3, and f^4 with the PDF.[7] The PDFs gradually deviate from the Gaussian function as y/b increases and exhibit a negatively skewed shape at $y/b = 1.5$.

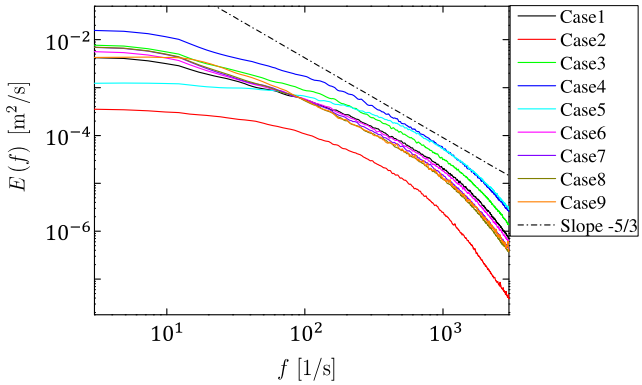

FIG. 5. Power spectra of velocity fluctuations.

B. Statistics of peak overpressure

Table II summarizes experimental results of the spherical shock wave interacting with the grid turbulence or turbulent wakes. Figure 7 plots the mean peak overpressure $\langle \Delta p \rangle$ divided by the atmospheric pressure P_∞ against (a) $d_{\rm i}$ and (b) $u_{\rm rms}$. Note that $\langle \Delta p \rangle / P_\infty$

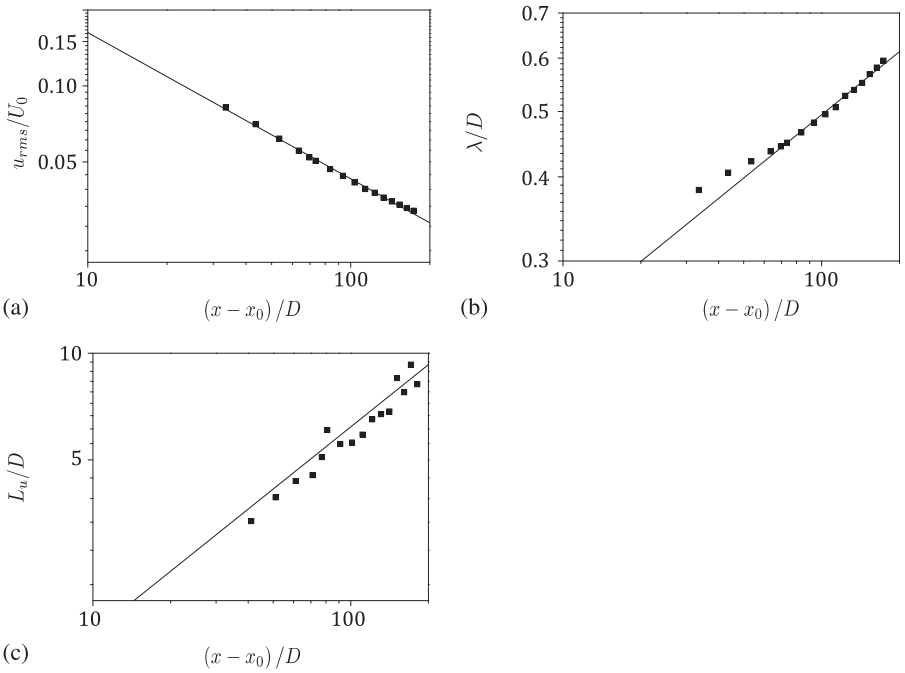

FIG. 4. Streamwise distributions of (a) $u_{\rm rms}/U_0$, (b) λ/D, and (c) L_u/D on the wake centerline. Solid lines are obtained by the least squares method: $u_{\rm rms}/U_0 = 0.62(x/D - 6.5)^{-0.58}$ in (a), $\lambda/D = 0.12(x/D - 6.5)^{0.311}$ in (b), and $L_u/D = 0.42(x/D - 6.5)^{0.58}$ in (c).

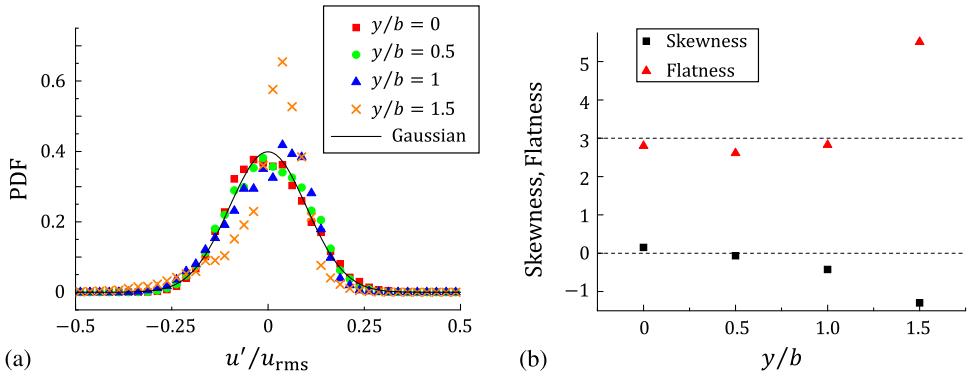

FIG. 6. (a) PDFs of streamwise velocity fluctuation u' in the cylinder wake (D = 10 mm) at different y locations and (b) skewness and flatness of streamwise velocity fluctuation. The results are obtained for the cylinder with D = 10 mm at x_s/D = 75.0.

TABLE II. Summary of experimental results of the spherical shock wave interacting with turbulent cylinder wakes.

Case	D (mm)	x_s (mm)	x_s/D	b (mm)	d_i (mm)	u_{rms} (m/s)	R_{max}	$\langle\Delta p\rangle/P_\infty$	$(\Delta p_{rms})_T/\langle\Delta p\rangle$
1	10	750	75.0	25.8	200	0.511	0.384	1.24×10^{-2}	1.65×10^{-2}
2	5	1500	300	22.7	208	0.203	0.166	1.26×10^{-2}	1.13×10^{-2}
3	12	654	54.5	26.1	201	0.658	0.415	1.23×10^{-2}	2.49×10^{-2}
4	15	565	37.6	27.7	201	0.870	0.491	1.21×10^{-2}	3.20×10^{-2}
5	5	285	57.0	10.6	85.8	0.539	0.114	1.25×10^{-2}	1.17×10^{-2}
6	12	900	75.0	31.6	240	0.529	0.475	1.21×10^{-2}	2.16×10^{-2}
7	15	1161	77.4	42.2	305	0.539	0.455	1.25×10^{-2}	2.94×10^{-2}
8	20	1500	75.0	53.5	400	0.512	0.397	1.25×10^{-2}	2.77×10^{-2}
9	Grid turbulence			...	562	0.549	0.235	1.25×10^{-2}	2.74×10^{-2}

is directly related to the mean shock Mach number by the Rankine–Hugoniot relation. Here, the cylinder wake experiments with $u_{rms} \approx 0.5$ m/s are shown in Fig. 7(a), while those with $d_i \approx 200$ mm are shown in Fig. 7(b). The results for the grid turbulence and laminar flow are also shown in the figures for comparison. For the cylinder wake experiments in Fig. 7(b), there is a clear trend of $\langle\Delta p\rangle/P_\infty$ decreasing with u_{rms} from the value of the shock wave that has propagated in a laminar flow. However, one cannot find a particular relation between $\langle\Delta p\rangle/P_\infty$ and d_i in Fig. 7(a). Values of $\langle\Delta p\rangle/P_\infty$ are similar for the shock waves that have propagated in the laminar flow and grid turbulence, and the grid turbulence hardly decreases the mean peak overpressure. One of the important differences between grid turbulence and cylinder wake is the influence of the mean velocity gradient. In fully developed turbulent wakes, u_{rms} scales with U_{def}.[7] The relation between $\langle\Delta p\rangle/P_\infty$ and u_{rms} in Fig. 7(b) implies that $\langle\Delta p\rangle/P_\infty$ decreases with the mean velocity defect. The decrease in $\langle\Delta p\rangle/P_\infty$ due to the nonuniform mean velocity profile in the wake can be explained by the deformation of the shock wave described in Fig. 8. The velocity of the shock wave movement can be expressed as the sum of the fluid velocity and the shock wave propagation velocity. Because of the velocity defect in the wake, the shock wave in the wake moves faster than in the freestream region.

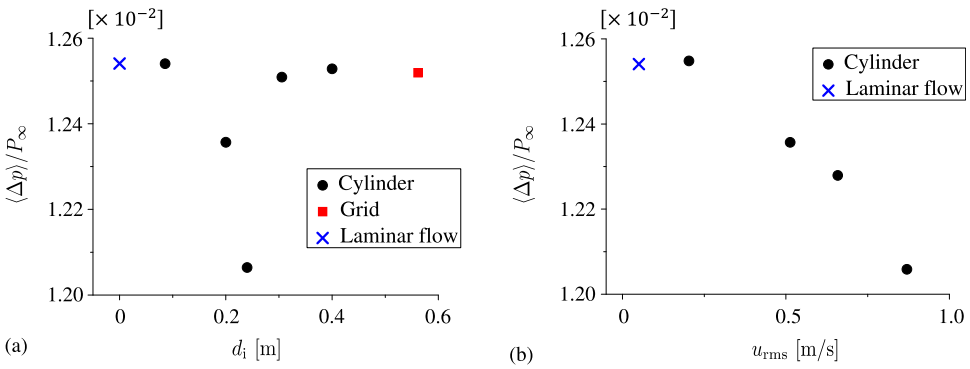

FIG. 7. Normalized mean overpressure $\langle\Delta p\rangle/P_\infty$ plotted against (a) interaction length d_i [case 1 and cases 5–9 with $u_{rms} \approx 0.5$ (m/s)] and (b) rms velocity fluctuation u_{rms} [cases 1–4 with $d_i \approx 0.2$ (m)].

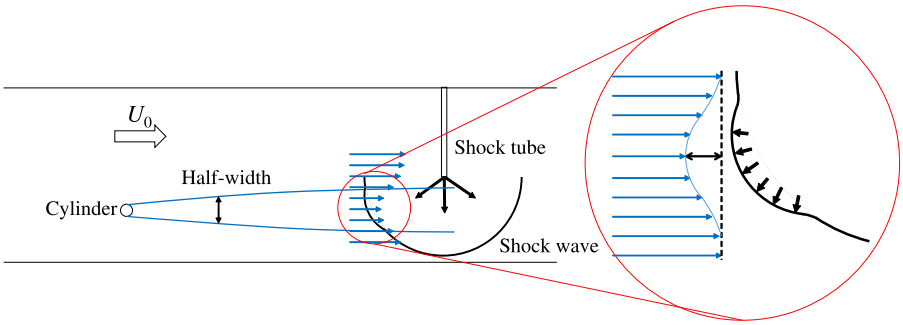

FIG. 8. Deformation of the spherical shock wave propagating in the cylinder wake.

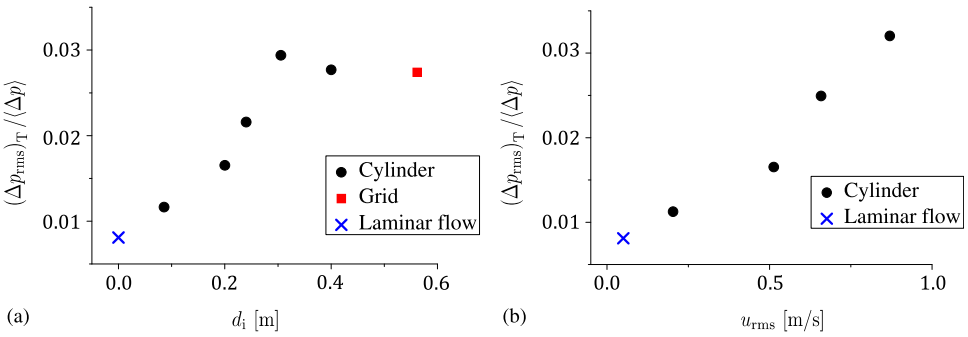

FIG. 9. Relative intensity of peak-overpressure fluctuation $(\Delta p_{\rm rms})_{\rm T}/\langle\Delta p\rangle$ plotted against (a) interaction length $d_{\rm i}$ [$u_{\rm rms} \approx 0.5$ (m/s), case 1, cases 5–9] and (b) rms velocity fluctuation $u_{\rm rms}$ [$d_{\rm i} \approx 0.2$ (m), cases 1–4].

This difference in the shock wave movement results in the deformation of the shock wave as shown in Fig. 8, where the shock wave tends to have a convex shape in the direction of the shock wave propagation. The convex shape causes a defocusing effect[23] that attenuates the shock wave strength and decreases the peak overpressure. Note that this explanation for $\langle\Delta p\rangle/P_\infty$ in the wake qualitatively agrees with the shock-tube experiments with a jet.[24] A normal shock wave in the jet was found to be weakened when it propagates in the same direction as the jet, where the jet with a larger streamwise velocity than the outside causes the convex shape in the direction of the shock propagation.

Figure 9(a) shows the relation between the relative intensity of peak overpressure fluctuation $(\Delta p_{\rm rms})_{\rm T}/\langle\Delta p\rangle$ with $d_{\rm i}$, where the results are taken from experiments with a cylinder wake or grid turbulence with $u_{\rm rms} \approx 0.5$ m/s. $(\Delta p_{\rm rms})_{\rm T}/\langle\Delta p\rangle$ increases with $d_{\rm i}$ between $d_{\rm i} = 0$ m and $d_{\rm i} = 0.3$ m, and the increase is saturated for $d_{\rm i} > 0.3$ m, for which $(\Delta p_{\rm rms})_{\rm T}/\langle\Delta p\rangle$ hardly depends on $d_{\rm i}$. Even though both the cylinder wake and grid turbulence used in Fig. 7(a) have $u_{\rm rms} \approx 0.5$ m/s, their influences on $(\Delta p_{\rm rms})_{\rm T}/\langle\Delta p\rangle$ are different for the cylinder wake with small $d_{\rm i}$. Numerical simulations of a planar shock wave propagating through homogeneous isotropic turbulence also showed that once the planar shock wave begins to interact with turbulence, the rms value of fluctuations in the pressure jump across the shock wave increases with time and then becomes independent of time after the shock wave propagates for a certain distance.[18] Our experimental results also confirm the same tendency: $(\Delta p_{\rm rms})_{\rm T}/\langle\Delta p\rangle$ increases with the interaction length d_i and becomes independent of $d_{\rm i}$ for large $d_{\rm i}$.

Figure 9(b) plots $(\Delta p_{\rm rms})_{\rm T}/\langle\Delta p\rangle$ against $u_{\rm rms}$, where the results for the cylinder wake are taken from the experiments with $d_{\rm i} \approx 200$ mm. The value of $d_{\rm i} \approx 200$ mm is in the regime in which $(\Delta p_{\rm rms})_{\rm T}/\langle\Delta p\rangle$ increases with $d_{\rm i}$ in Fig. 9(a). For a fixed value of $d_{\rm i} \approx 200$ mm, $(\Delta p_{\rm rms})_{\rm T}/\langle\Delta p\rangle$ monotonically increases with $u_{\rm rms}$. The increase in $(\Delta p_{\rm rms})_{\rm T}/\langle\Delta p\rangle$ with $u_{\rm rms}$ is also found in the interaction between the shock wave and grid turbulence, where the shock wave propagates only in the turbulent region.[21]

Figure 10 shows the probability density functions (PDFs) of the peak-overpressure fluctuation $\Delta p'/\Delta p_{\rm rms}$, where $\Delta p_{\rm rms} = \sqrt{\langle\Delta p^2\rangle - \langle\Delta p\rangle^2}$. The PDFs follow the Gaussian curve well in all cases. In numerical studies, the influences of turbulence on shock waves are often studied with the shock surface geometry. It was shown that the shock wave is wrinkled or broken when the turbulent Mach number is high in relation to the shock Mach number.[16]

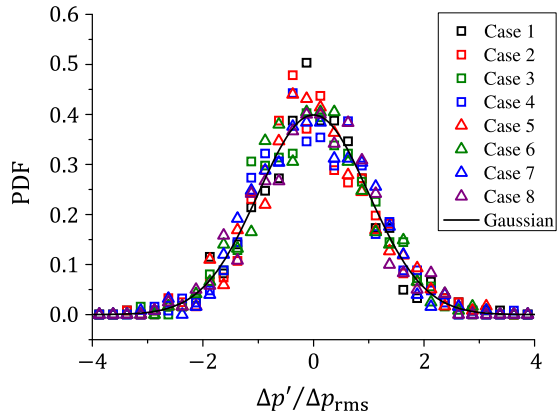

FIG. 10. Probability density functions of peak-overpressure fluctuations.

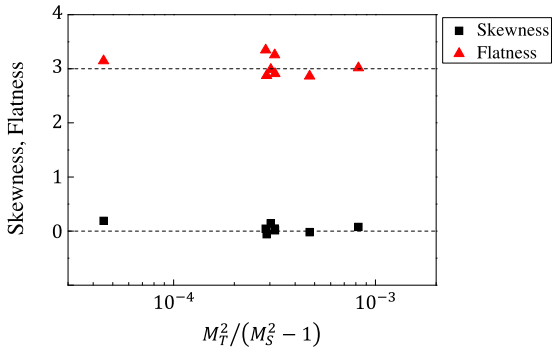

FIG. 11. Skewness and flatness of peak-overpressure fluctuations.

Criteria for the shock waves to be broken or wrinkled were proposed with several functions,[9,16] e.g., $M_T/(M_S-1)$ and $M_T^2/(M_S^2-1)$. It should be noted that $M_T^2/(M_S^2-1)$ can be interpreted as a measure of the ratio between the level of the pressure fluctuation induced by turbulence and the pressure jump across the shock wave. For the broken shock wave, the PDF of the density jump across a shock wave was found to deviate from the Gaussian function.[16] It should be noted that the peak overpressure $\Delta p'$ is almost proportional to the density jump fluctuation $\Delta\rho'$.[16] The skewness and flatness of $\Delta p'$ are plotted against $M_T^2/(M_S^2-1)$ in Fig. 11, where $M_T = u_{\rm rms}/a$ (a: sound speed). The values of $M_T^2/(M_S^2-1)$ in our experiments are not large enough for the turbulence to significantly change the shock surface geometry.[16] For the range of $M_T^2/(M_S^2-1)$ in our experiments, the skewness and flatness are close to the Gaussian values. Numerical simulations showed that a fluctuation in pressure jump of a planar shock wave is correlated with a velocity fluctuation of homogeneous isotropic turbulence,[18] where the PDF of the velocity fluctuation follows the Gaussian function. In contrast, the velocity fluctuation in the turbulent cylinder wake has a non-Gaussian PDF in the intermittent region (Fig. 6), where both turbulent and nonturbulent fluids intermittently appear.[48] Nevertheless, the shock wave interacting with the cylinder wake has a peak-overpressure fluctuation whose PDF is well approximated by the Gaussian function.

C. Correlation between velocity and peak-overpressure fluctuations

Figure 12 shows color contour plots of the correlation coefficient R between the velocity fluctuation and peak-overpressure fluctuation defined by Eq. (3) as a function of $(d, \Delta d)$. Positive values of the correlation are found in Fig. 12, except for case 2. Case 2 has the smallest rms velocity fluctuation, and the fluctuation of the peak overpressure induced by turbulence is also small. Therefore, the

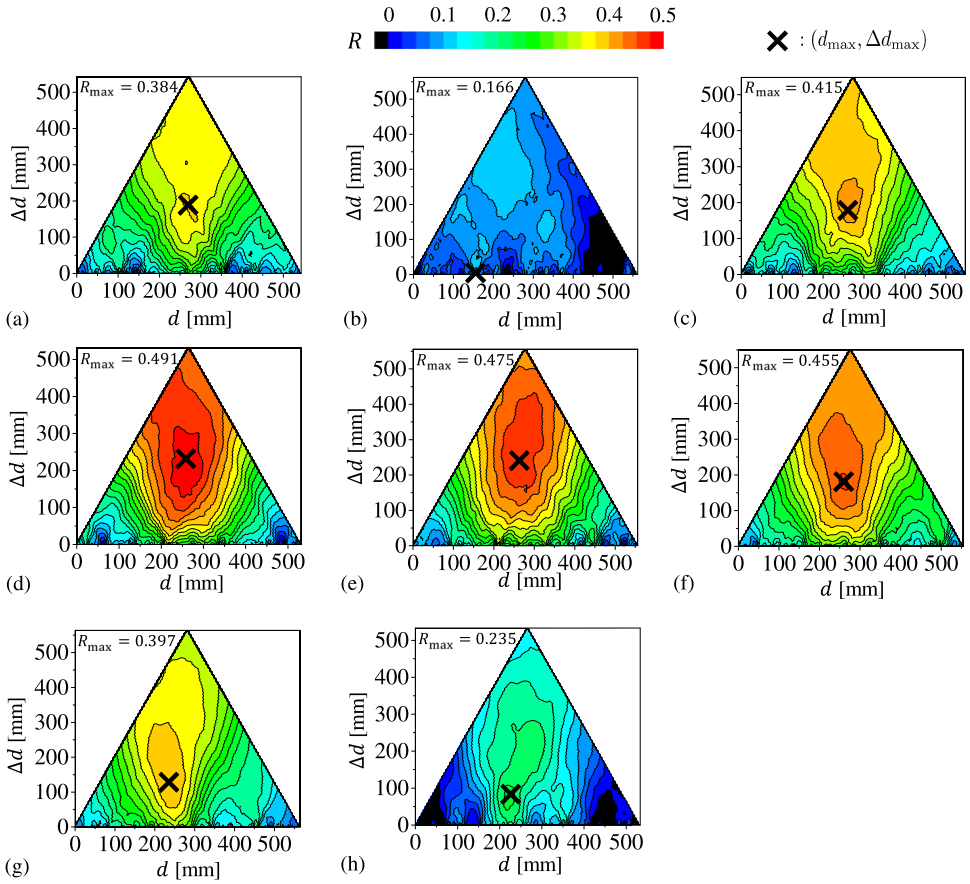

FIG. 12. Correlation coefficients $R(d, \Delta d)$ between peak-overpressure fluctuation and velocity fluctuation for (a) case 1, (b) case 2, (c) case 3, (d) case 4, (e) case 6, (f) case 7, (g) case 8, and (h) case 9. The crosses show $(d, \Delta d) = (d_{\max}, \Delta d_{\max})$, where R has a maximum value $R_{\max}$. Here, the color of the cross symbols does not represent the level of the correlation.

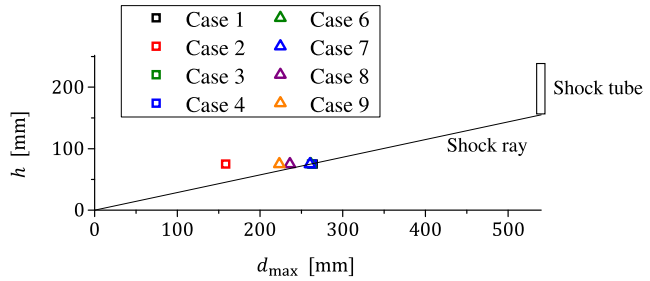

FIG. 13. Comparison of (d_{max}, h) with the shock ray toward the pressure transducer.

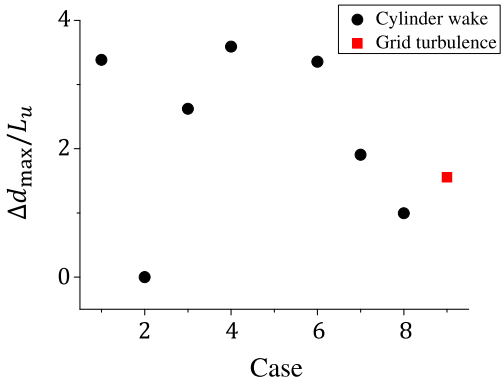

FIG. 14. Δd_{max} divided by the integral length scale L_u.

influence of the turbulent cylinder wake is not significant for case 2, and the weak correlation is obtained in Fig. 12(b). In each case, the maximum value of $R(d, \Delta d)$ is denoted as $R_{max}(d_{max}, \Delta d_{max})$, which is marked with cross symbols. The correlation becomes weaker for $(d, \Delta d) \neq (d_{max}, \Delta d_{max})$, and the velocity fluctuation at large scales $\Delta d_{max} = O(10^2$ mm) at the position of $d = d_{max}$ is strongly correlated with the pressure fluctuation. Figure 13 compares d_{max} with the shock ray from the open end of the shock tube to the pressure transducer. Here, h is the height from the measurement plate. One can see that the strongest correlation is obtained at the position near the shock ray. The deviation of d_{max} from the shock ray can be seen for case 2, and this is explained by the very weak correlation between the velocity fluctuation and peak-overpressure fluctuation.

Figure 14 shows Δd_{max} divided by the integral scale L_u. In the present experiments, Δd_{max} is the same order of the integral length scale of the turbulent cylinder wake. These results of (d_{max}, Δd_{max}) indicate that large-scale turbulent motions near the shock ray affect the peak overpressure.

Figure 15 plots maximum values of the correlation coefficient R_{max} against (a) d_i and (b) u_{rms}. The correlation becomes stronger as u_{rms} increases in Fig. 15(b). Dependence of R_{max} in Fig. 15(b) and $(\Delta p_{rms})_T$ in Fig. 9(b) on u_{rms} indicates that the influence of turbulence on the peak overpressure becomes stronger as u_{rms} increases. In Fig. 15(a), R_{max} peaks at d_i = 240 mm. From d_i = 200 mm to 240 mm, R_{max} increases with d_i, and the velocity fluctuation becomes more correlated with the peak-overpressure fluctuation for larger d_i. When d_i is very small, the shock wave stays in the turbulent region only for a short time. This may weaken the effects of turbulence on the shock wave for small d_i. For large $d_i \geq 300$ mm, R_{max} decreases with d_i. In this case, the shock wave propagates for a length long enough for $(\Delta p_{rms})_T/\langle \Delta p \rangle$ to be independent of d_i in Fig. 9(a). The correlation is obtained for the velocity at the center of the cylinder wake while the wake region below the centerline becomes wider with d_i. Therefore, in the case of large d_i, the influence of the velocity fluctuation on the centerline can be negated by fluctuations below the wake centerline. This causes the weaker correlation between the pressure and velocity fluctuation on the centerline.

The positive correlation means that the velocity fluctuation opposed to the shock wave propagating direction causes the increase in the peak overpressure, and vice versa. This result is consistent with previous experiments and numerical simulations of the shock/turbulence interaction,[18,38] where a two-point correlation was also investigated for the velocity fluctuation and the pressure jump of the shock wave. In these previous studies, the sign of the correlation was explained based on the shock wave deformation.[18,38] In our experiments, negative velocity fluctuations can locally create a convex shape in the direction of the shock wave propagation, and the defocusing effect for the convex shape decreases the peak overpressure (negative $\Delta p'$).[23] This effect is similar to the change in the mean peak overpressure caused by the mean velocity profile in Fig. 8. The opposite effect is expected for positive velocity fluctuations causing a concave shape of the shock wave with the focusing effect that amplifies the peak overpressure (positive $\Delta p'$).[23] These relations between the velocity fluctuation and $\Delta p'$ result in the positive correlation in Fig. 12. It was also found that there is a time delay for turbulent velocity fluctuations to change the pressure jump across the shock wave.[38] The effects of the turbulent velocity fluctuations gradually appear in the fluctuation of the pressure jump, and the fluid velocity

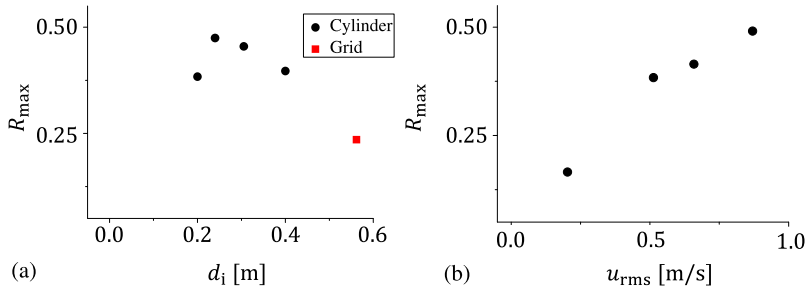

FIG. 15. Maximum values of the correlation coefficient R_{max} plotted against (a) interaction length d_i [case 1 and cases 5–9 with $u_{rms} \approx 0.5$ (m/s)] and (b) rms velocity fluctuation u_{rms} [cases 1–4 with $d_i \approx 0.2$ (m)].

fluctuation on the shock wave surface is weakly correlated with the pressure jump at the same instance.[18] This is why a strong correlation is found between the velocity fluctuation in the cylinder wake and the pressure measured on the wall.

IV. CONCLUSIONS

Wind tunnel experiments have been conducted for the spherical shock wave interacting with the turbulent cylinder wake, the grid turbulence, or the laminar flow. In the experiments with the wake, the shock wave, generated in the freestream, propagates through the turbulent cylinder wake and then its peak overpressure is measured outside the wake. The statistical properties of the peak overpressure of the spherical shock wave have been investigated in relation to the streamwise rms velocity fluctuation in the wake, u_{rms}, and the length of the turbulent region d_i through which the shock wave propagates. The present experiments demonstrate that inhomogeneity of turbulence is important in the shock/turbulence interaction as summarized below. Successful statistical models for the shock/turbulence interaction developed in future studies are expected to capture these effects of inhomogeneity in statistical properties of turbulence.

Pierce showed that the convex shape on the shock wave causes the defocusing effect that weakens the shock wave,[23] while the concave shape has the focusing effect that amplifies the peak overpressure.[23] The change in the peak overpressure in this study is also well explained based on Pierce's arguments. In the present experiments, the shock wave propagates in the opposite direction of the mean flow of the wake. The mean peak-overpressure is decreased by the wake, while the grid turbulence hardly changes the mean peak overpressure of the shock wave. The decrease in the mean peak overpressure by the wake is explained by the surface deformation of the shock wave caused by the mean velocity defect, under which the shock wave has a convex shape in the direction of the shock wave propagation. The correlation coefficient between the low-pass filtered streamwise velocity on the wake centerline and the peak overpressure fluctuation shows that the velocity fluctuation associated with large-scale turbulent motions on the shock ray has strong influences on the peak-overpressure fluctuation. The velocity fluctuation opposed to the direction of the shock wave propagation is positively correlated with the peak-overpressure fluctuation. This correlation can also be explained by the shock surface geometry caused by the velocity fluctuation. The velocity fluctuation opposed to the shock wave propagation can locally create the concave shape on the shock wave with the focusing effect. On the other hand, the convex shape with the defocusing effect can be created by the velocity fluctuation in the same direction as the shock wave propagation.

A series of experiments conducted for different d_i with a fixed value of u_{rms} have shown that the rms fluctuation of peak overpressure increases with d_i for small d_i while it becomes independent of d_i once d_i exceeds a certain value (300 mm in our experiments). The correlation coefficient in these experiments with various d_i has a peak value for d_i = 240 mm. The correlation becomes weaker for d_i < 240 mm, for which the length of the turbulent region is not large enough to affect the peak overpressure. For larger d_i, the turbulent flow region away from the wake centerline becomes wider, and the correlation between the velocity on the wake centerline and peak-overpressure can be weakened by the effects of these turbulent fluids. These results clearly show that one of the important parameters in the shock/turbulence interaction is the length of the turbulent region over which the shock wave propagates.

In the experiments with a fixed value of d_i, the rms fluctuation of peak overpressure monotonically increases with u_{rms}. The correlation between the velocity fluctuation and peak-overpressure fluctuation also becomes stronger with u_{rms}. Therefore, the turbulent effects on the shock wave tend to be stronger with u_{rms}. It has also been shown that the PDF of the peak-overpressure fluctuation is well approximated by a Gaussian function even though the shock wave has interacted with the turbulent wake, whose velocity fluctuation in the intermittent region has a non-Gaussian PDF.

ACKNOWLEDGMENTS

This work was supported by JSPS KAKENHI Grant Nos. 18J21758, 18H01367, 18H01369, and 18K13682. The authors would like to thank Professor A. Sasoh and Dr. K. Mori (Nagoya University) for their valuable comments. We would also like to thank Editage (www.editage.com) for English language editing.

REFERENCES

[1] D. J. Maglieri, "Some effects of airplane operations and the atmosphere on sonic-boom signatures," J. Acoust. Soc. Am. **39**, S36 (1966).
[2] K. J. Plotkin, "State of the art of sonic boom modeling," J. Acoust. Soc. Am. **111**, 530 (2002).
[3] H. Shen, "Sonic boom near-field predictions and its impact on the accuracy of ground signature predictions," J. Acoust. Soc. Am. **141**, 3565 (2017).
[4] M. Kanamori, T. Takahashi, Y. Makino, Y. Naka, and H. Ishikawa, "Comparison of simulated sonic boom in stratified atmosphere with flight test measurements," AIAA J. **56**, 2743 (2018).
[5] M.-M. Mac Low and R. S. Klessen, "Control of star formation by supersonic turbulence," Rev. Mod. Phys. **76**, 125 (2004).
[6] V. A. Thomas and R. J. Kares, "Drive asymmetry and the origin of turbulence in an ICF implosion," Phys. Rev. Lett. **109**, 075004 (2012).
[7] S. B. Pope, *Turbulent Flows* (Cambridge University Press, 2000).
[8] P. A. Davidson, *Turbulence: An Introduction for Scientists and Engineers* (Oxford University Press, 2004).
[9] S. Lee, S. K. Lele, and P. Moin, "Direct numerical simulation of isotropic turbulence interacting with a weak shock wave," J. Fluid Mech. **251**, 533 (1993).
[10] L. Jacquin, C. Cambon, and E. Blin, "Turbulence amplification by a shock wave and rapid distortion theory," Phys. Fluids **5**, 2539 (1993).
[11] J. Ryu and D. Livescu, "Turbulence structure behind the shock in canonical shock–vortical turbulence interaction," J. Fluid Mech. **756**, R1 (2014).
[12] D. A. Donzis, "Amplification factors in shock-turbulence interactions: Effect of shock thickness," Phys. Fluids **24**, 011705 (2012).
[13] D. A. Donzis, "Shock structure in shock-turbulence interactions," Phys. Fluids **24**, 126101 (2012).
[14] T. Kitamura, K. Nagata, Y. Sakai, A. Sasoh, and Y. Ito, "Rapid distortion theory analysis on the interaction between homogeneous turbulence and a planar shock wave," J. Fluid Mech. **802**, 108 (2016).
[15] J. Larsson and S. K. Lele, "Direct numerical simulation of canonical shock/turbulence interaction," Phys. Fluids **21**, 126101 (2009).
[16] J. Larsson, I. Bermejo-Moreno, and S. K. Lele, "Reynolds-and Mach-number effects in canonical shock-turbulence interaction," J. Fluid Mech. **717**, 293 (2013).
[17] D. Livescu and J. Ryu, "Vorticity dynamics after the shock–turbulence interaction," Shock Waves **26**, 241 (2016).
[18] K. Tanaka, T. Watanabe, K. Nagata, A. Sasoh, Y. Sakai, and T. Hayase, "Amplification and attenuation of shock wave strength caused by homogeneous isotropic turbulence," Phys. Fluids **30**, 035105 (2018).

[19]C. H. Chen and D. A. Donzis, "Shock–turbulence interactions at high turbulence intensities," J. Fluid Mech. **870**, 813 (2019).
[20]J. Keller and W. Merzkirch, "Interaction of a normal shock wave with a compressible turbulent flow," Exp. Fluids **8**, 241 (1990).
[21]A. Sasoh, T. Harasaki, T. Kitamura, D. Takagi, S. Ito, A. Matsuda, K. Nagata, and Y. Sakai, "Statistical behavior of post-shock overpressure past grid turbulence," Shock Waves **24**, 489 (2014).
[22]T. Kitamura, K. Nagata, Y. Sakai, A. Sasoh, and Y. Ito, "Changes in divergence-free grid turbulence interacting with a weak spherical shock wave," Phys. Fluids **29**, 065114 (2017).
[23]A. D. Pierce, "Statistical theory of atmospheric turbulence effects on sonic-boom rise times," J. Acoust. Soc. Am. **49**, 906 (1971).
[24]H. S. Ribner, P. J. Morris, and W. H. Chu, "Laboratory simulation of development of superbooms by atmospheric turbulence," J. Acoust. Soc. Am. **53**, 926 (1973).
[25]J. H. Kim, A. Sasoh, and A. Matsuda, "Modulations of a weak shock wave through a turbulent slit jet," Shock Waves **20**, 339 (2010).
[26]C. B. da Silva, J. C. R. Hunt, I. Eames, and J. Westerweel, "Interfacial layers between regions of different turbulence intensity," Annu. Rev. Fluid. Mech. **46**, 567 (2014).
[27]T. Watanabe, Y. Sakai, K. Nagata, Y. Ito, and T. Hayase, "Turbulent mixing of passive scalar near turbulent and non-turbulent interface in mixing layers," Phys. Fluids **27**, 085109 (2015).
[28]J. Eisma, J. Westerweel, G. Ooms, and G. E. Elsinga, "Interfaces and internal layers in a turbulent boundary layer," Phys. Fluids **27**, 055103 (2015).
[29]A. Cimarelli, G. Cocconi, B. Frohnapfel, and E. De Angelis, "Spectral enstrophy budget in a shear-less flow with turbulent/non-turbulent interface," Phys. Fluids **27**, 125106 (2015).
[30]T. S. Silva and C. B. da Silva, "The behaviour of the scalar gradient across the turbulent/non-turbulent interface in jets," Phys. Fluids **29**, 085106 (2017).
[31]X. Wu, J. M. Wallace, and J.-P. Hickey, "Boundary layer turbulence and freestream turbulence interface, turbulent spot and freestream turbulence interface, laminar boundary layer and freestream turbulence interface," Phys. Fluids **31**, 045104 (2019).
[32]R. Jahanbakhshi, N. S. Vaghefi, and C. K. Madnia, "Baroclinic vorticity generation near the turbulent/non-turbulent interface in a compressible shear layer," Phys. Fluids **27**, 105105 (2015).
[33]R. Jahanbakhshi and C. K. Madnia, "Entrainment in a compressible turbulent shear layer," J. Fluid Mech. **797**, 564 (2016).
[34]R. Nagata, T. Watanabe, and K. Nagata, "Turbulent/non-turbulent interfaces in temporally evolving compressible planar jets," Phys. Fluids **30**, 105109 (2018).
[35]L. Agostini, L. Larchevêque, and P. Dupont, "Mechanism of shock unsteadiness in separated shock/boundary-layer interactions," Phys. Fluids **27**, 126103 (2015).
[36]Y. Zhuang, H. Tan, X. Li, Y. Guo, and F. Sheng, "Evolution of coherent vortical structures in a shock wave/turbulent boundary-layer interaction flow," Phys. Fluids **30**, 111702 (2018).
[37]T. Kitamura, K. Nagata, Y. Sakai, A. Sasoh, O. Terashima, H. Saito, and T. Harasaki, "On invariants in grid turbulence at moderate Reynolds numbers," J. Fluid Mech. **738**, 378 (2014).
[38]K. Inokuma, T. Watanabe, K. Nagata, A. Sasoh, and Y. Sakai, "Finite response time of shock wave modulation by turbulence," Phys. Fluids **29**, 051701 (2017).
[39]K. Inokuma, T. Watanabe, K. Nagata, and Y. Sakai, "Statistics of overpressure fluctuations behind a weak shock wave interacting with turbulence," Phys. Fluids **31**, 085119 (2019).
[40]I. Wygnanski and H. Fiedler, "Some measurements in the self-preserving jet," J. Fluid Mech. **38**, 577 (1969).
[41]R. C. Deo, G. J. Nathan, and J. Mi, "Similarity analysis of the momentum field of a subsonic, plane air jet with varying jet-exit and local Reynolds numbers," Phys. Fluids **25**, 015115 (2013).
[42]T. Watanabe, Y. Sakai, K. Nagata, Y. Ito, and T. Hayase, "Enstrophy and passive scalar transport near the turbulent/non-turbulent interface in a turbulent planar jet flow," Phys. Fluids **26**, 105103 (2014).
[43]T. Watanabe, T. Naito, Y. Sakai, K. Nagata, and Y. Ito, "Mixing and chemical reaction at high Schmidt number near turbulent/nonturbulent interface in planar liquid jet," Phys. Fluids **27**, 035114 (2015).
[44]L. Schwer, "Air blast reflection ratios and angle of incidence," in *Proceedings of the 11th European LS-DYNA Conference* (DYNAmore, 2017), pp. 9–11.
[45]G. Ben-Dor, *Shock Wave Reflection Phenomena* (Springer, 1992).
[46]Y. Zhou and R. A. Antonia, "Convection velocity measurements in a cylinder wake," Exp. Fluids **13**, 63 (1992).
[47]H. Osaka, H. Yamada, I. Nakamura, Y. Kuwata, and Y. Kageyama, "The structure of a turbulent wake behind a cruciform circular cylinder: 2nd report, the streamwise development of turbulent flow field," Bull. JSME **26**, 521 (1983).
[48]J. C. LaRue and P. A. Libby, "Temperature fluctuations in the plane turbulent wake," Phys. Fluids **17**, 1956 (1974).